Glass Transition and Re-entranl Melting in a Polydisperse Hard-Sphere Fluid

doi: 10.1063/1.2204460

Glass Transition and Re-entrant Melting in a Polydisperse Hard-Sphere Fluid

Michio Tokuyama* and Yayoi Terada*

*Institute of Fluid Science, Tohoku University, Sendai 980-8577, Japan

Abstract. Extensive molecular dynamics simulations are performed for a hard-sphere fluid at 6% polydispersity. The simulation results are then analyzed based on the mean-field theory proposed recently by Tokuyama (*Physica A* **364**, 23-62 (2006)). The phase diagram and the dynamic behavior are investigated fully in each phase. It is then found that as the volume fraction ϕ is increased, a supercooled liquid phase appears at the supercooled point $\phi_\beta (\simeq 0.5524)$ and a transition from supercooled liquid to crystal then occurs at the melting volume fraction $\phi_m^{(1)} (\simeq 0.5625)$. As ϕ is further increased, a transition from crystal to supercooled liquid (re-entrant melting) is also observed at the second melting volume fraction $\phi_m^{(2)} (\simeq 0.5770)$ within a waiting time $t_w = 7 \times 10^4 t_0$, where t_0 is a time for a particle to move over a distance of a particle radius with an average velocity. The glass transition is thus predicted to occur at the glass transition volume fraction $\phi_g (\simeq 0.6005)$. The various aspects obtained in our study is quite similar to those in the experiment for the suspension of hard spheres, including the logarithmic growth of the mean-square displacement in fast-β stage, the non-singular behavior of the long-time self-diffusion coefficient, and the non divergence of any characteristic times, such as the α- and β-relaxation times.

Keywords: Glass transition, Hard spheres, Re-entrant Melting, Solid-liquid transition, Supercooled liquid
PACS: 64.70.Pf, 64.70.Dv, 61.20.Gy, 83.10.Mj

INTRODUCTION

The suspension of hard-sphere colloids is experimentally known to cause the glass transition at 6% size polydispersity [1]. This transition is considered to be mainly due to the long-range hydrodynamic interactions between colloids. In fact, we have recently shown by performing the Brownian-dynamics simulation [2] that there exists no glass transition in the suspension with 6% polydispersity if the hydrodynamic interactions are completely neglected but there occurs only a first-order phase transition from liquid to crystal at the melting volume fraction ϕ_m. Hence it has been believed for long times that this is also true for the hard-sphere fluid which consists of hard spheres with the same size polydispersity. However, we point out that the equilibrium phase behavior of the hard-sphere fluid must be different from that of the suspension without hydrodynamic interactions in the following two reasons. The first reason is that the long-time self-diffusion coefficient $D_S^L(\phi)$ for the hard-sphere fluid is lower than that of the suspension for all values of the volume fraction ϕ, whose difference coincides with the short-time self-diffusion coefficient $D_S^S(\phi)$ obtained by the short-time hydrodynamic interactions [2]. The second reason is that the existence of a supercooled liquid state is predicted for $\phi_\beta \le \phi < \phi_m$ in the hard-sphere fluid, where ϕ_β is a supercooled point over which the supercooled state appears. Hence a transition from a supercooled liquid to crystal is expected at ϕ_m, while in the suspension there is no such transition but a transition from liquid to crystal at ϕ_m. Thus, the 6% polydispersity can change the equilibrium phase behavior in the hard-sphere fluid but not in the suspension. In fact, the possibility of re-entrant melting (transition from crystal to liquid) is suggested by free energy calculations [3] for the system of hard spheres with small size polydispersity. In this paper, therefore, we perform extensive molecular-dynamics simulations for a hard-sphere fluid with 6% polydispersity and investigate the equilibrium phase behavior for higher volume fractions by analyzing the simulation results from a unified point of view proposed recently [4].

The mean-square displacement is used to distinguish each phase together with the radial distribution function $g(r)$. In a liquid region it grows linearly in time for a long time, while in a crystal region it becomes constant for a long time. As the volume fraction ϕ is increased, we thus observe the re-entrant melting at a higher volume fraction. In fact, there exist five types of phases [5]. The first is a liquid phase [L] for $\phi < \phi_\beta (\simeq 0.5524)$. The second is a supercooled-liquid phase [SI] for $\phi_\beta \le \phi < \phi_m^{(1)}$, where $\phi_m^{(1)} (\simeq 0.5625)$ denotes the melting volume fraction at which the first-order phase transition from supercooled liquid to crystal occurs. The supercooled state is suggested by the mean-field analyses and is confirmed by the split of the second peak of $g(r)$. The third is a crystal phase [C] for $\phi_m^{(1)} \le \phi \le \phi_m^{(2)}$, where $\phi_m^{(2)} (\simeq 0.5770)$ denotes the second melting volume fraction at which the re-entrant melting from crystal to supercooled liquid is

CP832, *Flow Dynamics, The Second International Conference on Flow Dynamics*
edited by M. Tokuyama and S. Maruyama

observed. The fourth is a supercooled-liquid phase [SII] for $\phi_m^{(2)} < \phi < \phi_g$, where the second peak of $g(r)$ shows a split and $\phi_g (\simeq 0.6005)$ is a glass transition volume fraction. The glass phase [G] is also expected to exist for $\phi_g \leq \phi$. Although the results similar to the above have already been reported in the previous paper [5], we here present more precise results obtained recently for a sufficiently long waiting time of order $7 \times 10^4 t_0$ than the previous one of order $5 \times 10^4 t_0$, where the first melting point $\phi_m^{(1)} \simeq 0.5630$ and the second melting point $\phi_m^{(2)} \simeq 0.5715$ obtained in Ref. [5] are corrected as 0.5625 and 0.5770, respectively.

We show that the dynamical behavior in the hard-sphere fluid is very similar to that in the real system of the suspension. In fact, the long-time self-diffusion coefficient $D_S^L(\phi)$ can be obtained by using the mean-square displacement in a liquid region. It is thus shown that D_S^L is described by exactly the same non-singular function of ϕ as that predicted theoretically to explain a recent experiment for the suspension by van Megen et al [1], if both ϕ axis and D_S^L axis are adjusted properly. Hence no divergence is also found for any characteristic times, such as the α-relaxation time and the β-relaxation time. Thus, we confirm from a new point of view that there exist remarkable similarities between the hard-sphere fluid and the suspension of hard-sphere colloids for higher volume fractions in various aspects, except the existence of the crystal state in the hard-sphere fluid.

We begin in Sec. II by reviewing the mean-field theory proposed recently [4], which is used in the present paper. In Sec. III we perform the molecular-dynamics simulation for hard-sphere fluids and analyze the simulation results by using the mean-field theory. We conclude in Sec. IV with a summary.

MEAN-FIELD EQUATIONS

In this section we briefly summarize and discuss the mean-field equations for the mean-square displacement in hard-sphere fluids and concepts which we use in this paper.

We discuss the three-dimensional molecular system, which contains N particles with mass m_i and radius a_i in the total volume V at a constant temperature T, where the mass m_i is proportional to a_i^3. The distribution $f(a_i)$ of particle radius a_i is assumed to obey a Gaussian distribution given by

$$f(a_i) = \frac{1}{(2\pi)^{1/2} s a} \exp[-\frac{(a_i/a-1)^2}{2s^2}] \qquad (1)$$

with standard deviation s over the range $1-3s \leq a_i \leq 1+3s$, where $s = (\overline{a_i^2}/a^2 - 1)^{1/2}$. Here $a = \overline{a_i}$, where the overbar indicates an average over $f(a_i)$. The main interaction of this system is only a direct interaction between particles, where the particles are described by Newtonian equations. The control parameter is given by the volume fraction $\phi = (4\pi a^3 N/3V)(1+3s^2)$, where $s = 0$ for a monodisperse case and $s \neq 0$ for a polydisperse case. The relevant variables are given by a set of the position vectors of particles, $\{\boldsymbol{X}_1(t), ..., \boldsymbol{X}_N(t)\}$, where $\boldsymbol{X}_i(t)$ denotes a position vector of the ith particle at time t.

The mean-square displacement $M_2(t)$ is given by

$$M_2(t) = \frac{1}{N} \sum_{i=1}^{N} < [\boldsymbol{X}_i(t) - \boldsymbol{X}_i(0)]^2 >, \qquad (2)$$

where the brackets denote the equilibrium ensemble average. As shown in Ref. [2], for the molecular systems it obeys the following mean-field equation:

$$\frac{d}{dt} M_2(t) = 2d D_S^L(\phi) + 2d \left[\frac{v_0^2}{d} t - D_S^L(\phi) \right] e^{-M_2(t)/\ell(\phi)^2}, \qquad (3)$$

where $\ell(\phi)$ is a free length to be determined and d the spatial dimensionality. Here $v_0(T) (= \sqrt{3k_B T/m})$ denotes the average velocity of a particle, where T is the temperature and $m (= \overline{m_i})$ the average mass. The formal solution is given by

$$M_2(t) = \ell^2 \ln \left[1 + \frac{1}{18} (\frac{\ell v_0}{D_S^L})^2 \{ e^{6D_S^L t/\ell^2} - 1 - 6D_S^L t/\ell^2 \} \right]. \qquad (4)$$

The particles move freely by ballistic motion, up to a time scale of order t_f, where $t_f(\phi) (= \ell/v_0)$ is a free time for a particle to move over a distance of order ℓ. Hence the solution (4) suggests the following asymptotic forms:

$$M_2(t) \simeq \begin{cases} M_0^M(t) = \ell^2 \ln[1 + (t/t_f)^2] & \text{for } t \leq t_f, \\ 6D_S^L t & \text{for } t_L \leq t, \end{cases} \qquad (5)$$

where $t_L (= a^2/D_S^L)$ is a long-diffusion time for a particle to diffuse over a distance of order a with the diffusion coefficient D_S^L. Hence we have two stages. The first is an early stage [E] for $t \ll t_f$, where $M_2(t)$ grows as $M_2(t) \simeq (v_0 t)^2$ and the ballistic motion dominates the system. The second is a late stage [L] for $t_L \leq t$, where $M_2(t)$ grows linearly in time as $M_2(t) \simeq 6D_S^L t$ and the long-time diffusion dominates the system. Equation (3) thus turns out to describe the dynamics of a crossover from the ballistic motion characterized by v_0 to the long-time self-diffusion process characterized by D_S^L.

Near the glass transition point ϕ_g, there exists another time stage, the so-called β-relaxation stage [β] for $t_f \ll t \ll t_L$. In fact, between two time scales, t_f and t_L, one can further define two more time scales, t_γ and t_β where $t_\gamma \ll t_\beta$. As discussed in Ref. [4], in order to find them,

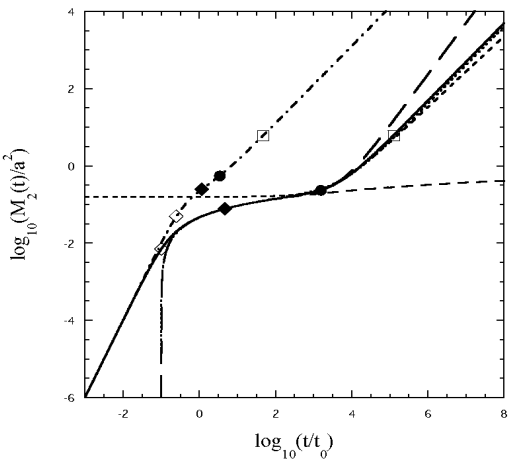

FIGURE 1. A log-log plot of the mean-square displacement $M_2(t)$ versus time. The solid line indicates the result for $\phi = 0.590$, where $\ell = 0.1$ and $D_S^L = 7.943 \times 10^{-6}$ and the dot-dashed line for $\phi = 0.505$, where $\ell = 0.246$ and $D_S^L = 0.0209$. The long-dashed line indicates $M_0^M(t)$, the dotted line the growth by Eq. (10) with $b_\gamma^M(0.590) \simeq 1.0028, B_1(0.590) \simeq 1.8 \times 10^{-4}$, and $t_\gamma \simeq 4.65$, and the long-long-dashed line by Eq. (11) with $b_\beta^M(0.590) \simeq 1.33014$, $B_2(0.590) \simeq 0.042$, and $t_\beta \simeq 1541$. The symbols indicate the time scales: t_f (open diamond), t_γ (filled diamond), t_β (filled circle), and t_L (open square). The dashed line indicates the power-law growth of von Schweidler type given by Eq. (12).

it is convenient to calculate the logarithmic derivatives given by

$$\varphi_1^M(t,\phi) = \frac{\partial}{\partial \log t} \log |M_2(t) - M_0^M(t)|, \quad (6)$$

$$\varphi_2^M(t,\phi) = \frac{\partial}{\partial \log t} \varphi_1^M(t). \quad (7)$$

Then, $\varphi_2^M(t) = 0$ gives two time roots, t_γ and t_β, which reveal two fairly flat regions for $\phi > \phi_s$;

$$\varphi_1^M = \begin{cases} b_\beta^M(\phi) & \text{at } t = t_\beta, \\ b_\gamma^M(\phi) & \text{at } t = t_\gamma, \end{cases} \quad (8)$$

where $b_\beta^M(\phi)$ and $b_\gamma^M(\phi)$ are time exponents to be determined. Here the times t_β and t_γ are shown to be approximately described by

$$t_\beta \simeq 1.2 \frac{\ell^2}{D_S^L}, \; t_\gamma \simeq 1.2 t_0 \left(\frac{t_f t_\beta}{t_0^2} \right)^{1/4}, \quad (9)$$

respectively, where $t_0 = a/v_0$ and $t_f \ll t_\gamma \ll t_\beta \ll t_L$. Here the volume fraction ϕ_s denotes the β point above which the β stage appears since $b_\gamma^M = b_\beta^M$ and $t_\gamma = t_\beta$ at $\phi = \phi_s$. Thus, we find two time stages for $\phi > \phi_s$; a fast β-relaxation stage [β_f] for $t_f \ll t \ll t_\beta$ and a slow β-relaxation stage [β_s] for $t_\gamma \ll t \ll t_L$. Here t_β is identical to the so-called β-relaxation time, while t_γ is a time scale to describe a plateau. By expanding $M_0^M(t)$ in powers of $\ln(t/t_\gamma)$, in stage [β_f], we obtain the asymptotic form

$$\begin{aligned} M_2(t) &\simeq M_0^M(t) + B_1(\phi)(t/t_\gamma)^{b_\gamma^M} \\ &\simeq \ell^2 \Big\{ \ln\big(1 + (\frac{t_\gamma}{t_f})^2\big) \\ &+ 2\ln(\frac{t}{t_\gamma}) + \ell^{-2} B_1(\phi) (\frac{t}{t_\gamma})^{b_\gamma^M} \Big\}, \end{aligned} \quad (10)$$

where $B_1(\phi)$ is a positive constant to be determined. Since $B_1/\ell^2 \ll 1$ near ϕ_g, $M_2(t)$ is mostly dominated by the logarithmic growth given by $\ln(t/t_\gamma)$ around t_γ. In stage [β_s], we also obtain the asymptotic form

$$\begin{aligned} M_2(t) &\simeq M_0^M(t) + B_2(\phi)(t/t_\beta)^{b_\beta^M} \\ &\simeq \ell^2 \Big\{ \ln\big(1 + (\frac{t_\beta}{t_f})^2\big) \\ &+ 2\ln(\frac{t}{t_\beta}) + \ell^{-2} B_2(\phi) (\frac{t}{t_\beta})^{b_\beta^M} \Big\}, \end{aligned} \quad (11)$$

where $B_2(\phi)$ is a positive constant to be determined. Since $B_2/\ell^2 > 1$ near ϕ_g, $M_2(t)$ is mostly dominated by the power-law growth given by $(t/t_\beta)^{b_\beta^M}$ around t_β. It is shown that as ϕ approaches to ϕ_g, both exponents b_γ^M and b_β^M decrease and become constant beyond ϕ_g as $b_\beta^M = 1.3301$ and $b_\gamma^M = 1.0$. Especially, the exponent b_γ^M shows an inflection point at which the slope $db_\gamma^M/d\phi$ becomes minimum and the exponent b_β^M nearly reduces to 1.3301. Hence this inflection point must be a supercooled point ϕ_β over which the supercooled liquid phase appears. This is confirmed later by analyzing the simulation results and also by calculating the other physical quantities, such as the radial distribution function and the self-part of the dynamic susceptibility. For earlier times $M_2(t)$ thus obeys a logarithmic growth in time, while for later times it obeys a power-law growth of a super-diffusion type with $b_\beta^M > 1.0$. Here we note that since $b_\beta^M > 1.0$, this power-law growth is different from the so-called von Schweidler type with the exponent less than 1.0. In Fig. 1, a log-log plot of $M_2(t)$ is shown for different volume fractions, $\phi = 0.505$ and 0.590. For comparison, the following power-law growth of von Schweidler type is also shown at $\phi = 0.590$:

$$M_2(t) = 10^{-0.8} + 0.085(t/t_\beta)^{0.92}. \quad (12)$$

As ϕ increases, the separations between the characteristic times $\{t_i\}$ become large and the logarithmic growth dominates the system around t_γ in the fast β stage, while both equations (11) and (12) well describe the system around t_β in the slow β stage.

Near the glass transition point ϕ_g, the self-intermediate scattering function $F_S(k,t)$ can be written as [6]

$$\begin{aligned} F_S(k,t) &= <\exp[-i\boldsymbol{k}\cdot\{\boldsymbol{X}_i(t)-\boldsymbol{X}_i(0)\}]> \\ &\simeq \exp\left[-k^2\frac{M_2(t)}{6}+\frac{1}{2}k^4\left(\frac{M_2(t)}{6}\right)^2\alpha_2(t)\right] \\ &\quad +O(k^6) \end{aligned} \tag{13}$$

with the three dimensional non-Gaussian parameter

$$\alpha_2(t)=\frac{3}{5}\frac{M_4(t)}{M_2(t)^2}-1, \tag{14}$$

where $M_4(t)$ is the mean-fourth displacement given by

$$M_4(t)=<([\boldsymbol{X}_i(t)-\boldsymbol{X}_i(0)]^2)^2>. \tag{15}$$

When $\alpha_2(t)$ is negligibly small, the characteristic time stages of $F_S(k,t)$ are identical to those of $M_2(t)$. This type is mostly seen in the suspension of neutral hard spheres [1]. When $\alpha_2(t)$ is not negligible, however, a new time stage, the so-called α-relaxation stage [α] for $t_\beta \ll t \ll t_L$, appears around t_α in the dynamics of $F_S(k,t)$, in addition to the three time stages of $M_2(t)$, where the α-relaxation time t_α is determined by the peak position of the non-Gaussian parameter $\alpha_2(t)$ and satisfies $t_\beta \ll t_\alpha \ll t_L$. This type is seen in most of the systems.

SIMULATIONS ON HARD-SPHERE FLUIDS

We here perform a molecular-dynamics simulation on a hard-sphere fluid. The system consists of 10976 hard spheres with radius a_i and mass m_i in a cubic box of volume V at a constant temperature T, where the standard deviation s is given by $s=0.06$.

The position vector $\boldsymbol{X}_i(t)$ of ith particle obeys the Newton equation

$$m_i\frac{d^2}{dt^2}\boldsymbol{X}_i(t)=\sum_{j\neq i}\boldsymbol{F}(\boldsymbol{X}_{ij}(t)), \tag{16}$$

where $\boldsymbol{F}(\boldsymbol{X}_{ij})$ denotes the force due to the elastic binary collisions between particles i and j and $\boldsymbol{X}_{ij}=\boldsymbol{X}_i-\boldsymbol{X}_j$. We first scale the position vector $\boldsymbol{X}_i$ with radius a, time t with $t_0(=a/v_0)$, and D_S^L with av_0. Then, we solve Eq. (16) under periodic boundary and appropriate initial conditions together with the momentum and the energy conservation laws. The simulations start from two kinds of nonequilibrium initial states. The first is a disordered initial state which shows a random configuration and is obtained by using the Jodrey and Tory's algorithm [7]. The other is an ordered initial state which shows a face-centered-cubic configuration. Then, we wait for a long time enough to reach a final state in which the mean-square displacement $M_2(t)$ grows linearly in time in a liquid phase or becomes constant in a crystal phase. The waiting time t_w is chosen to be $7\times10^4 t_0$ for all volume fractions here. The typical relaxation times $t_L(\phi)$ and t_β are listed in Table 1. If the waiting time is much longer than t_L, the final state is considered to be almost in equilibrium. By choosing this final state as an initial state, therefore, we repeat the simulations again. If the whole time behavior of $M_2(t)$ coincides with a previous one, one can then conclude that all the results are in an equilibrium state. Here we should note from Table 1 that the systems with the volume fractions higher than 0.580 do not reach an equilibrium state yet within our waiting time but we repeat the same procedure as the above to get the results near an equilibrium state.

TABLE 1. The relaxation times $t_L(\phi)$ and t_β for different volume fractions.

ϕ	t_L/t_0	t_β/t_0
0.500	4.30×10^1	3.14
0.525	7.99×10^1	4.79
0.540	1.43×10^2	7.58
0.550	2.47×10^2	11.85
0.560	5.10×10^2	20.16
0.580	2.00×10^4	370.17
0.582	2.50×10^4	415.62
0.586	7.08×10^4	922.15
0.600	4.57×10^5	3981.07

Depending on the values of the volume fractions, there exist five phase regions at $s=0.06$ [5]; a stable liquid region for $\phi<\phi_f(s)$, a metastable region I for $\phi_f(s)\le\phi<\phi_m^{(1)}(s)$, a stable crystal region for $\phi_m^{(1)}(s)\le\phi\le\phi_m^{(2)}$, a metastable region II for $\phi_m^{(2)}<\phi<\phi_g$, and a glass region for $\phi_g\le\phi$, where ϕ_f, $\phi_m^{(1)}$, $\phi_m^{(2)}$, and ϕ_g are the so-called freezing volume fraction, the melting volume fractions, and the glass transition volume fraction, respectively. We note here that a crystal to liquid first-order phase transition is also observed at $\phi_m^{(2)}(s)$ in addition to a conventional liquid to crystal first-order phase transition at $\phi_m^{(1)}(s)$. From the simulations we find $\phi_f(0.06)\simeq 0.5300$, $\phi_m^{(1)}(0.06)\simeq 0.5625$, and $\phi_m^{(2)}(0.06)\simeq 0.5770$. In a liquid region the system reaches an equilibrium liquid state after a long time, even if one starts from different initial states. In metastable regions the final equilibrium state depends on from which nonequilibrium initial state one starts, a disordered state or an ordered state. In

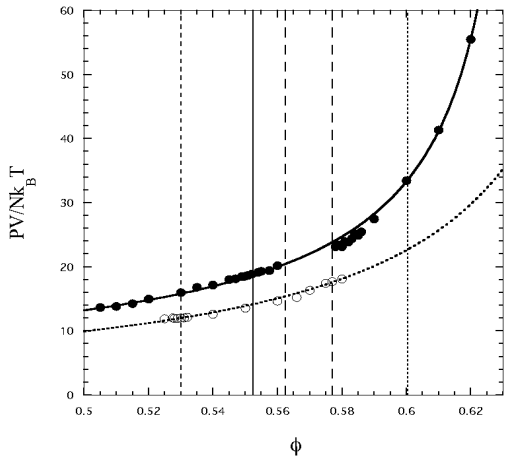

FIGURE 2. Pressure versus volume fraction. The open circles indicate the simulation results in a crystal state and the filled circles in a liquid state. The solid line indicates the fitting singular function given by Eq. (19) for the liquid branch and the dotted line Eq. (20) for the crystal branch. The vertical dashed line indicates the freezing point ϕ_f, the vertical solid line the supercooled point ϕ_β, the vertical long-dashed lines the melting points $\phi_m^{(i)}$, and the vertical dotted line the glass transition point ϕ_g.

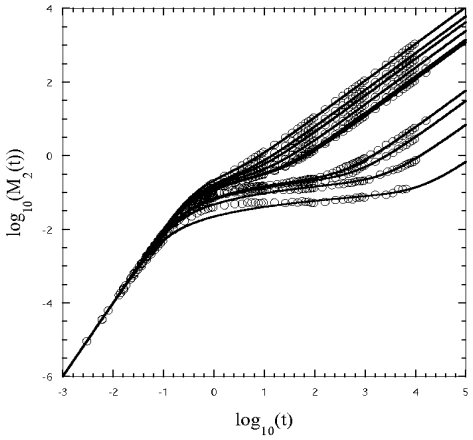

FIGURE 3. A log-log plot of $M_2(t)$ versus time at $s = 0.06$ in the liquid state for different volume fractions ϕ=0.5100, 0.5300, 0.5400, 0.5500, 0.5575, 0.5600, 0.5780, 0.5800, 0.5860, and 0.6100 (from left to right). The solid lines indicate the mean-field results given by Eq. (9) and the open circles the simulation results.

fact, the system reaches a metastable liquid state after a long time if one starts from a disordered state, while it reaches a metastable crystal state after a long time if one starts from an ordered state. We note here that even after long computational times, the system still remains in each metastable state. In a crystal region it reaches an equilibrium crystal state after a long time irrespectively of initial states. The pressure $P(\phi)$ can be obtained by using the Virial theorem as

$$\frac{PV}{Nk_BT} = 1+\frac{1}{3k_BT}\sum_{i=1}^{N}\sum_{j\neq i}<\boldsymbol{X_i}\cdot\boldsymbol{F}(\boldsymbol{X}_{ij})>, \quad (17)$$

$$= 1-\frac{2}{3Nk_BT}\frac{1}{\tau}\sum_{collisions}\frac{m_im_j}{m_i+m_j}\boldsymbol{V}_{ij}\cdot\boldsymbol{X}_{ij}, \quad (18)$$

where $\sum_{collisions}$ denotes the summation over all collisions between particles i and j, which occur during an arbitrary time τ, and $\boldsymbol{V}_{ij} = (d/dt)\boldsymbol{X}_{ij}$. In Fig. 2 the phase diagram is shown in the pressure-volume fraction plane. There exist two branches; the liquid branch and the crystal branch. The liquid branch starts at a small volume fraction and ends at the so-called random close packing fraction $\phi_{RCP}(s)$, where there is no liquid state between $\phi_m^{(1)}$ and $\phi_m^{(2)}$. The crystal branch starts at $\phi_f(s)$ and ends at the close packing fraction $\phi_{CP}(s)$. Here $\phi_{RCP}(0.06) \simeq 0.64$ and $\phi_{CP}(0.06) \simeq 0.69$ [8]. The liquid branch and the crystal branch are well described by the singular functions

$$\frac{PV}{Nk_BT} = 4.3\left(1-\frac{\phi}{\phi_{RCP}(s)}\right)^{-0.74}, \quad (19)$$

$$\frac{PV}{Nk_BT} = 2.4\left(1-\frac{\phi}{\phi_{CP}(s)}\right)^{-1.1}, \quad (20)$$

respectively. The singular behavior for the liquid branch is somewhat similar to previous numerical results [9, 10, 11] but there are some discrepancies for the singular exponent between them.

In Fig. 3, the simulation results for $M_2(t)$ are shown in liquid states for different volume fractions. Up to $\phi = 0.5800$, the simulation results are well described by the mean-field equation given by Eq. (3). As mentioned before, however, the results for volume fractions higher than $\phi = 0.582$ do not fit that equation in the fast β-relaxation stage because they do not reach an equilibrium state yet within a waiting time $7\times10^4 t_0$. In Fig. 4, the typical equilibrium simulation results are compared with the mean-field results at ϕ =0.5600 and 0.5780.

At the late stage for $t \geq t_L$ both in a stable liquid state and in a metastable liquid state the mean-square displacement $M_2(t)$ grows linearly in time as

$$M_2(t) \simeq 6D_S^L(\phi)t. \quad (21)$$

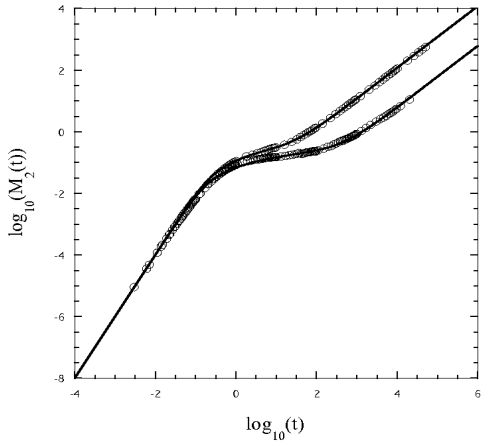

FIGURE 4. A log-log plot of $M_2(t)$ versus time at $s = 0.06$ in the equilibrium supercooled-liquid state for ϕ= 0.5600 [S_I] and 0.5780 [S_{II}]. The details are the same as in Fig. 3.

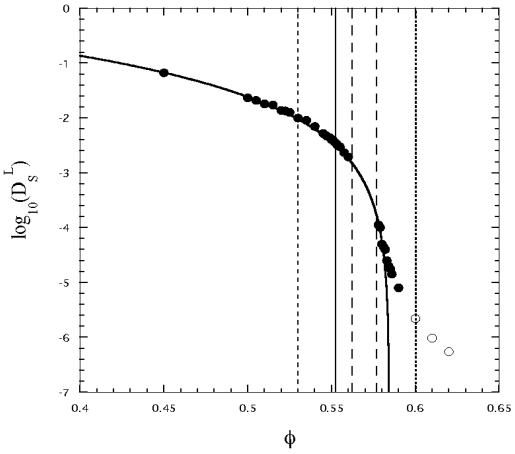

FIGURE 5. A log plot of $D_S^L(\phi)$ versus ϕ. The filled circles indicate the simulation results and the open circles the theoretical prediction. The solid line the singular function given by Eq. (22). The details are the same as in Fig. 2.

Hence one can obtain the values of $D_S^L(\phi)$ by using Eq. (21) and the simulation results. A log plot of D_S^L versus ϕ is thus shown in Fig. 5. Here the results for the volume fractions higher than 0.6 are predicted by using the mean-field theory since those results do not reach a late stage yet. As discussed in Ref. [4], the results are approximately described by the singular function

$$\frac{D_S^L(\phi)}{av_0} = \frac{D_S^S(\phi)/D_0}{1+\frac{D_S^S(\phi)}{D_0}\left(\frac{\phi}{\phi_c}\right)\left(1-\frac{\phi}{\phi_c}\right)^{-2}}, \qquad (22)$$

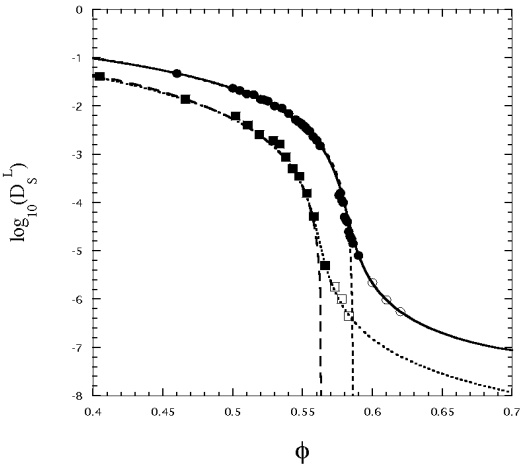

FIGURE 6. Non-singular behavior of the long-time self-diffusion coefficient $D_S^L(\phi)$. The solid line indicates the resultant non-singular function for the hard-sphere fluid and the dotted line the non-singular function for the suspension from Ref. [13, 14]. The filled circles indicate the simulation results and the open circles the prediction by the mean-field theory. The filled squares indicate the experimental results for the suspension from Ref. [1] and the open squares the theoretical prediction. The dashed line indicates the singular function given by Eq.(22) and the long-dashed line Eq. (24).

where and $\phi_c(0.06) \simeq 0.5845$. Here $D_S^S(\phi)$ denotes the short-time self-diffusion coefficient for the hard-sphere colloids due to the short-time hydrodynamic interactions [12] and $D_0(= k_BT/6\pi\eta a)$ a diffusion coefficient of a single colloid. Near the singular point ϕ_c, $D_S^L(\phi)$ behaves as

$$\frac{D_S^L(\phi)}{av_0} \simeq \left(1-\frac{\phi}{\phi_c}\right)^2. \qquad (23)$$

As discussed in the previous paper [4], however, the simulation results deviate from the singular function beyond ϕ_c and seem to obey a non-singular function. In fact, one can find such a non-singular function by using the non-singular function proposed for the experimental data for the suspension of hard spheres [4, 13], which is shown together with the experimental results obtained by van Megen et al [1] in Fig. 6. In order to find a non-singular function for the simulation results from the experimental one, one can use the singular functions by which the experimental results and the simulation results are approximately described. In fact, the experimental results are also shown to obey the singular function given by [4]

$$D_S^L(\phi) = D_S^S(\phi)\frac{1-1.2\phi}{1+\frac{D_S^S(\phi)}{D_0}\left(\frac{\phi}{\phi_c^S}\right)\left(1-\frac{\phi}{\phi_c^S}\right)^{-2}}, \qquad (24)$$

where $\phi_c^S = 0.564$. Here the factor 1.2ϕ in the numerator results from the coupling between the direct interactions

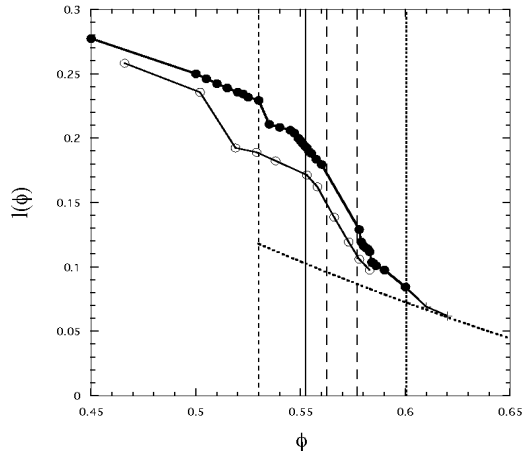

FIGURE 7. A plot of $\ell(\phi)$ versus ϕ. The filled circles indicate the fitting results. The open circles indicate the experimental results for the suspension from Ref. [13]. The symbols (+) indicate the results predicted by the mean-field theory. The dotted line indicates the free length ℓ_c given by Eq. 25. The solid lines are guides to the eye. The details are the same as in Fig. 5.

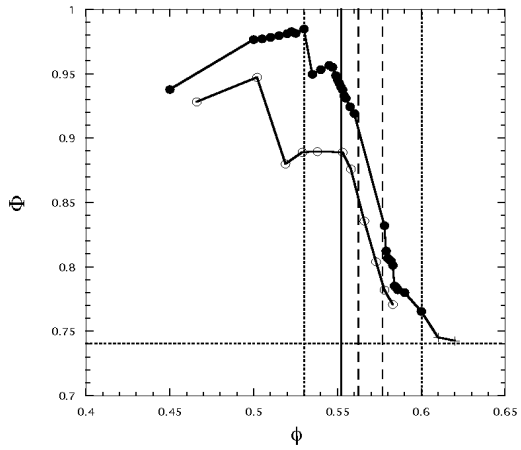

FIGURE 8. A plot of Φ versus ϕ. The dotted line indicates Φ_c. The details are the same as in Fig. 7.

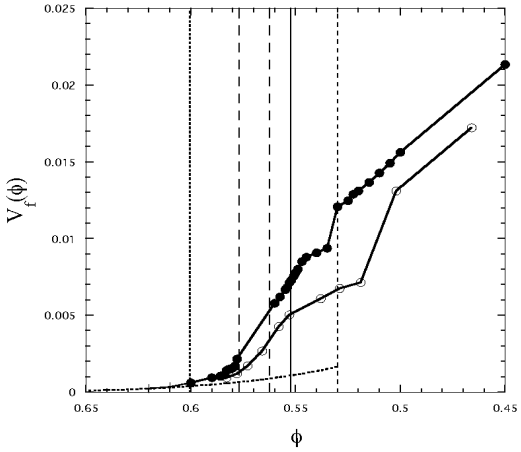

FIGURE 9. A plot of $V_f(\phi)$ versus ϕ. The details are the same as in Fig. 7.

and the short-range hydrodynamic interactions. On the other hand, the simulation results obey the singular function given by Eq. (22). In order to shift the non-singular function proposed for the experimental data to the simulation results, therefore, one may first transform the volume fraction ϕ into $\phi+\phi_c-\phi_c^S$ and then divide the non-singular function by the factor $(1-1.2\phi)$. The resulting non-singular function is turned out to describe the simulation results very well (see Fig. 6). Thus, this suggests that a non-singular behavior is common feature near the glass transition [4, 14]. The glass transition is also expected to occur around $\phi_g=0.6005$ for the hard-sphere fluid since $\phi_g=\phi_g^S+\phi_c-\phi_c^S$, where $\phi_g^S=0.58$ [1].

The free length $\ell(\phi)$ is shown in Fig. 7. Here the fitting value of the adjustable parameter ℓ is determined in such a way that the mean-field result of $M_2(t)$ coincides with the simulation result at $t=t_\gamma$. The free length ℓ_c in the crystal branch of the monodisperse hard-sphere fluid is given by

$$\ell_c=\frac{1}{\sqrt{2}}\left(\frac{2\pi}{3\phi}\right)^{1/3}-1. \tag{25}$$

In Fig. 7, it is also shown for comparison. As ϕ increases, ℓ decreases monotonically and changes a little bit around $\phi_f(=0.5300)$. Above $\phi_\beta(\simeq 0.5524)$, it starts to decrease steeply. We note here that the ϕ dependence of ℓ is very similar to that obtained experimentally for the suspension of hard spheres [4, 13]. This is more clearly seen by introducing the free volume fraction Φ by

$$\Phi=\phi(1+\ell/a)^3. \tag{26}$$

In Fig. 8, the free volume fraction Φ is shown together with the results for the suspension. The fraction $\Phi_c(=\phi(1+\ell_c/a)^3)$ for the crystal is also shown, where $\Phi_c=\sqrt{2}\pi/6\simeq 0.74048$. The ϕ dependence of the simulation results is thus shown to be very similar to the experimental results. In fact, as ϕ increases, Φ increases for small volume fractions and then starts to decrease up to the freezing volume fraction ϕ_f, at which the birth and death of the clustering starts. After ϕ_f, it increases again and then starts to decrease drastically beyond the super-

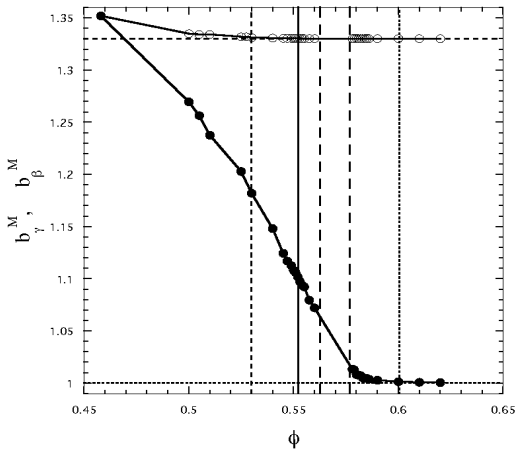

FIGURE 10. A plot of time exponents $b_\beta^M(\phi)$ and $b_\gamma^M(\phi)$ versus ϕ. The filled circles stand for b_γ^M and the open circles for b_β^M. The horizontal dashed line indicates $b_\beta^M = 1.3301$ and the horizontal dotted line $b_\gamma^M = 1.0$. The solid lines are guides to the eye. The details are the same as in Fig. 5.

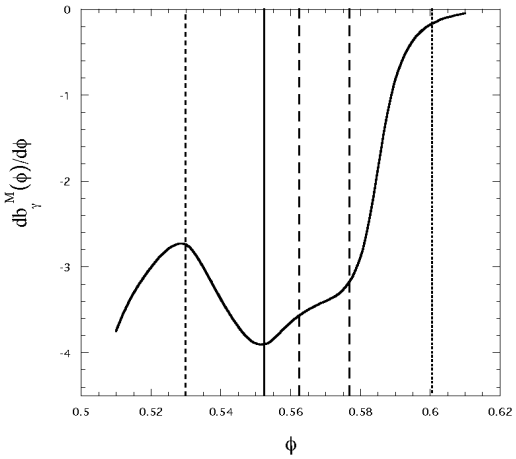

FIGURE 11. A plot of the slope $db_\gamma^S(\phi)/d\phi$ versus ϕ. The solid line indicates the mean-field result obtained by using the fitting functions for D_S^L and ℓ. The details are the same as in Fig. 5.

cooled point ϕ_β, over which the clustering occurs everywhere. The free volume V_f must be proportional to ℓ^3, since ℓ is proportional to $M_2(t)^{1/2}$ at time $t = \ell^2/(6D_S^L)$. Hence the function $V_f(\phi)(= \ell^3)$ is also shown in Fig. 9. For comparison, the results for the suspension are also plotted. The volume fraction dependence of V_f for the hard-sphere fluid is very similar to that obtained for the real colloidal suspension.

In Fig. 10 the time exponents $b_\beta^M(\phi)$ and $b_\gamma^M(\phi)$ are also shown. We find $\phi_s(0.06) \simeq 0.4580$, over which the β stage appears. As ϕ increases, both exponents decrease and become constant beyond ϕ_g as $b_\beta^M = 1.3301$ and $b_\gamma^M = 1.0$. Especially, as is shown in Fig. 11, the exponent b_γ^M shows a inflection point at $\phi = 0.5524$ where the slop $db_\gamma^M/d\phi$ becomes minimum and b_β^M nearly reduces to 1.3301. As discussed in the previous paper [4], this inflection point denotes a supercooled point ϕ_β over which the supercooled liquid phase appears. Here we note that the second inflection point around $\phi = 0.530$ at which the slop becomes maximum is expected to be a freezing point ϕ_f. In order to check it, however, one should wait a time longer than $5 \times 10^4 t_0$.

In Fig. 12 the non-Gaussian parameter $\alpha_2(t)$ is shown for different volume fractions in liquid states. The peak height of $\alpha_2(t)$ at t_α becomes larger than 1.0 for $\phi > \phi_m^{(2)}$, while it is smaller than 1.0 for $\phi < \phi_m^{(1)}$. Here we should note that the supercooled region [SI] exists for $\phi_\beta \le \phi < \phi_m^{(1)}$, although the peak height $\alpha_2(t_\alpha)$ is

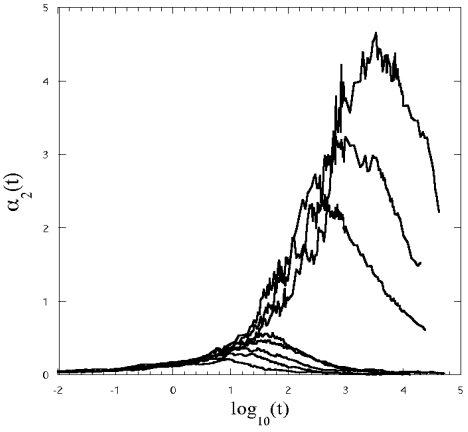

FIGURE 12. Non-Gaussian parameter $\alpha_2(t)$ versus time for different volume fractions ϕ=0.5200, 0.5400, 0.5500, 0.5575, 0.5600, 0.5780, 0.5800, and 0.5860 (from left to right).

not larger than 1.0. The same situation as this is seen for the real colloidal suspension of hard spheres, where $\alpha_2(t)$ is negligible for all volume fractions [1]. In Fig. 13 the characteristic times $\{t_f, t_\gamma, t_\beta, t_\alpha, t_L\}$ are then plotted versus ϕ. The so-called α-relaxation time t_α, which is a peak positions of $\alpha_2(t)$, is also shown. As ϕ is increased, t_α, t_β, t_γ, and t_L increase steeply above ϕ_β, while t_f decreases. We note here that no divergence is found in any characteristic times for higher volume fractions.

The supercooled point ϕ_β can be also confirmed by

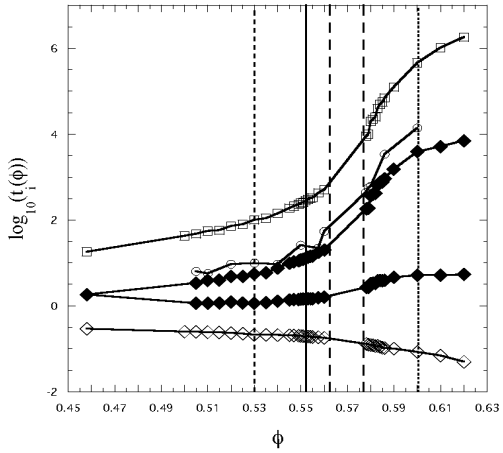

FIGURE 13. A log plot of the characteristic times $\{t_i(\phi)\}$. The open squares stand for t_L, open circles for t_α, filled circles for t_β, the filled diamonds for t_γ, and the open diamonds for t_f. The solid lines are guides to the eye. The details are the same as in Fig. 5.

calculating the other physical quantities, such as a radial distribution function $g(r)$ and a self part of the dynamic susceptibility $\chi_S^{"}(k,\omega)$. First, we discuss the radial distribution function $g(r)$ given by

$$g(r) = \frac{V}{N^2} < \sum_{i=1}^{N} \sum_{j \neq i} \delta(\boldsymbol{r} + \boldsymbol{X}_j - \boldsymbol{X}_i) > \qquad (27)$$

Figs. 14(a), (b), and (c) show the typical spatial configurations in different phases; (a) the liquid phase at $\phi = 0.5200$, 0.5300, and 0.5400, (b) the supercooled liquid phase at ϕ =0.5600, 0.5790, and 0.5800, and (c) the crystal phase at ϕ =0.5675, 0.5700, and 0.5750. In the supercooled phase the second peak of $g(r)$ shows a split, while it shows just a single peak in the liquid phase. In the crystal phase the peak positions of $g(r)$ coincide with those of a face-centered cubic (FCC) packing up to the fifth peak. Thus, one can find five phase regions, starting from a nonequilibrium random configuration initially. The first is a liquid region [L] for $\phi < \phi_\beta$. The second is a supercooled-liquid region I [S_I] for $\phi_\beta \leq \phi < \phi_m^{(1)}$. The third is a crystal region [C] for $\phi_m^{(1)} \leq \phi \leq \phi_m^{(2)}$. The fourth is a supercooled-liquid region II [S_{II}] for $\phi_m^{(2)} < \phi < \phi_g$. The last is a glass region [G] for $\phi_g \leq \phi$. Here $\phi_\beta(0.06) \simeq 0.5524$, $\phi_m^{(1)}(0.06) \simeq 0.5625$, $\phi_m^{(2)}(0.06) \simeq 0.5770$, and $\phi_g \simeq 0.6005$. This is a first evidence by simulations to show the existence of a phase transition from a supercooled liquid to a crystal for a hard-sphere fluid with polydispersity $s = 0.06$, although this kind of transition is already known experimentally

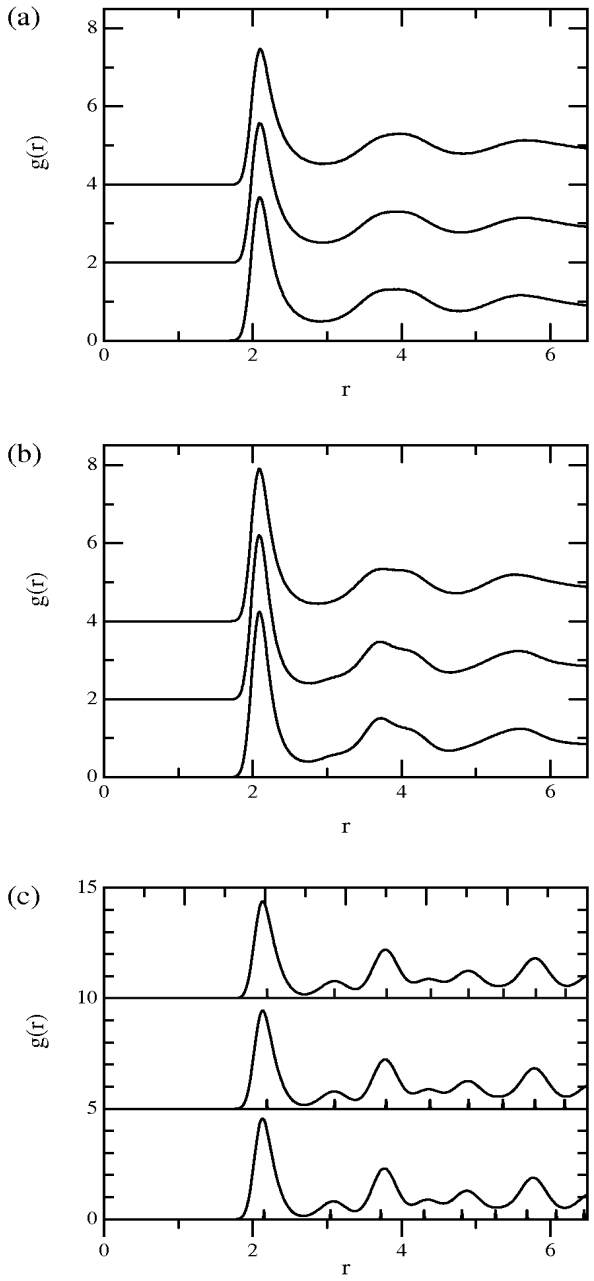

FIGURE 14. The radial distribution function $g(r)$ in different phases; (a) the liquid phase at $\phi = 0.5200$, 0.5300, and 0.5400 (from top to bottom), (b) the supercooled liquid phase at ϕ =0.5600, 0.5790, and 0.5800 (from top to bottom), and (c) the crystal phase at ϕ =0.5675, 0.5700, and 0.5750 (from top to bottom). The vertical lines indicate the theoretical results for a FCC crystal. The upper curves are shifted vertically for the sake of clarity.

for water, and also the occurrence of re-entrant melting, a first-order phase transition from crystal to supercooled liquid, around $\phi = 0.5770$.

Next we discuss the self-part of the dynamic susceptibility $\chi_S^{"}(k,\omega)$ given by

$$\chi_S^{"}(k,\omega) = \omega \int_0^\infty F_S(k,t)\cos(\omega t)dt. \qquad (28)$$

Since $\alpha_2(t)$ is much smaller than 1.0 for $\phi < \phi_m^{(1)}$, one can calculate $\chi_S^{"}(k,\omega)$ without $\alpha_2(t)$ in the supercooled region [S_I]. Then, using Eqs. (4) and (13), one finds

$$F_S(k,t) = \left[1 + \frac{1}{18}\left(\frac{\ell v_0}{D_S^L}\right)^2\left\{e^{6D_S^L t/\ell^2} - 1 - 6D_S^L t/\ell^2\right\}\right]^{-\frac{(k\ell)^2}{6}}. \qquad (29)$$

In Fig. 15 the susceptibility $\chi_S^{"}(k,\omega)$ is shown at the peak position $k = 3.4$ of $S(k)$ for different volume fractions, where $S(k)$ denotes the static structure factor. In region [S_I] the shoulder appears clearly around the β frequency ω_β, while in region [S_{II}] the double peaks, α peak and β peak, appear around ω_L and ω_γ, respectively, where $\omega_i = 2\pi/t_i$. We note here that if one calculates $\chi_S^{"}(k,\omega)$, including $\alpha_2(t)$, one would also expect double peaks even in region [S_I] since those are found in the real colloidal suspension although $\alpha_2(t)$ is small. In fact, this would be confirmed by the fact that, as is shown in Fig. 16, the simulation results for $F_S(k,t)$ differ from the mean-field results calculated by Eq. (29) at the α-relaxation stage around t_α, even though the non-Gaussian parameter $\alpha_2(t)$ is small in region [S_I].

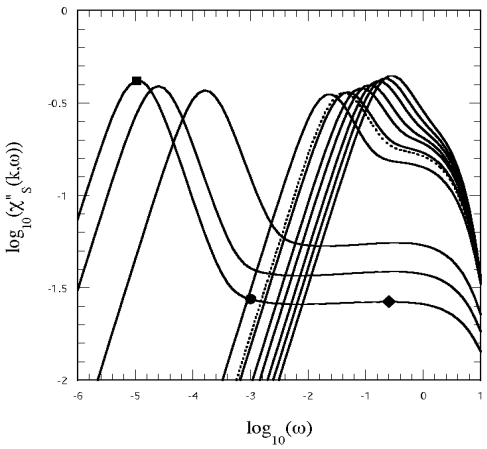

FIGURE 15. A log-log plot of $\chi_S^{"}(k,\omega)$ versus frequency at $s = 0.06$ and $k = 3.4$ for different volume fractions ϕ =0.5000, 0.5100, 0.5200, 0.5300, 0.5400, 0.5500, 0.5524, 0.5600, 0.5860, 0.6000, and 0.6100 (from right to left). The solid lines indicate the mean-field results given by Eq. (28) and the dotted line for $\phi_\beta = 0.5524$. The symbols indicate the characteristic frequencies: ω_γ (filled diamond), ω_β (filled circle), and ω_L (filled square).

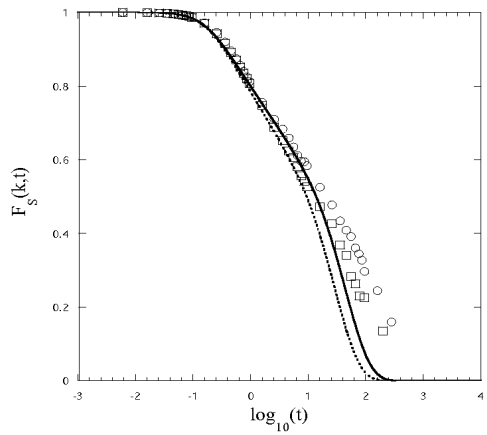

FIGURE 16. A plot of the self-intermediate scattering function $F_S(k,t)$ versus time in the supercooled liquid region [S_I] at ϕ =0.5550 (open squares) and 0.5600 (open circles). The dotted and solid lines indicate the mean-field results given by Eq. (29) at $\phi = 0.5550$ and 0.5600, respectively.

SUMMARY

We have studied the equilibrium phase diagram of a hard-sphere fluid with 6% size polydispersity. This was done not only by performing the extensive molecular-dynamics simulations but also by analyzing the simulation results by the mean-field theory from a unified point of view. We have shown that starting from two kind of nonequilibrium initial configurations, a random configuration and a FCC configuration, the system reaches two different final states, a liquid state and a crystal state, within the waiting time $t_w = 7 \times 10^4 t_0$. Depending on the values of the volume fraction, there exist five phase regions. The first is a stable liquid region for $\phi < \phi_f$, where the system reaches the liquid state irrespectively of initial configurations. The second is a metastable region I for $\phi_f \le \phi < \phi_m^{(1)}$. The system reaches the liquid state if one starts from the random configuration, while it reaches the crystal state if one starts from the FCC configuration. Depending on ϕ, there exists two different metastable liquid states. One is a liquid state for $\phi_f \le \phi < \phi_\beta$. The other is a supercooled state for $\phi_\beta \le \phi < \phi_m^{(1)}$. The third is a stable crystal region for $\phi_m^{(1)} \le \phi \le \phi_m^{(2)}$, where the system reaches the crystal state irrespectively of initial

configurations. The fourth is a metastable region II for $\phi_m^{(2)} < \phi < \phi_g$. The system reaches the supercooled liquid state if one starts from the random configuration, while it reaches the crystal state if one starts from the FCC configuration. The last is a glass region for $\phi_g \leq \phi$. The system reaches the glass state if one starts from the random configuration, while it reaches the crystal state if one starts from the FCC configuration. We have thus shown that as the volume fraction ϕ is increased, transition from supercooled liquid to crystal first occurs at $\phi \simeq 0.5625$ and the re-entrant melting from crystal to supercooled liquid is then observed at $\phi \simeq 0.5770$.

In a liquid state, we have obtained the long-time self-diffusion coefficient $D_S^L(\phi)$ by using the mean-square displacement $M_2(t)$ and shown that $D_S^L(\phi)$ obeys exactly the same non-singular function as that proposed to explain the experimental results for the suspension of hard-sphere colloids. We have also examined the volume fraction dependence of the adjustable parameter $\ell(\phi)$ and the characteristic times $t_L(\phi)$, $t_\alpha(\phi)$, $t_\beta(\phi)$, $t_\gamma(\phi)$, and $t_f(\phi)$. We have thus found that there is no divergence in any characteristic times at the glass transition. By comparing different glass transitions through the mean-field theory from a unified point of view, we have predicted that the supercooled liquid phase appears at $\phi \simeq 0.5524$ and the glass transition occurs at $\phi \simeq 0.6005$. Those were also confirmed by checking the other physical quantities, such as the radial distribution function $g(r)$ and the self-part of the dynamic susceptibility $\chi_S^{\cdot\cdot}(k,\omega)$.

Finally, we comment on a waiting time t_w. In order to equilibrate the system, it must be sufficiently longer than the relaxation time t_L. Hence we took $t_w = 7 \times 10^4 t_0$ here. This is long enough to equilibrate the system for $\phi \leq 0.582$ since $t_w >> t_L(\phi = 0.582) \simeq 2.50 \times 10^4 t_0$. Within this time, we have thus shown that the metastable liquid state can exist for $\phi_m^{(2)} < \phi$. However, it is not clear yet at the present stage whether the crystallization occurs or not for much longer waiting times. This will be discussed elsewhere together with the details near the glass transition.

ACKNOWLEDGMENTS

This work was partially supported by Grants-in-aid for Science Research with No. 14540348 from Ministry of Education, Culture, Sports, Science and Technology of Japan. Numerical computations for this work were performed on the Origin 2000 machine at the Institute of liquid Science, Tohoku University.

REFERENCES

1. W. van Megen, T. C. Mortensen, S. R. Williams, and J. Müller, *Phys. Rev. E* **58**, 6073-6085 (1998).
2. M. Tokuyama, H. Yamazaki, and Y. Terada,*Phys. Rev. E* **67**, 062403-1-4 (2003);
3. P. Bartlett and P. B. Warren, *Phys. Rev. Lett.* **82**, 1979-1982 (1999).
4. M. Tokuyama, *Physica A*, **364**, 23-62 (2006).
5. M. Tokuyama and Y. Terada, *J. Phys. Chem. B* **109**, 21357-21363 (2005).
6. B. R. A. Nijboer and A. Rahman, *Physica (Amsterdam)* **32**, 415-432 (1966).
7. W. S. Jodrey and E. M. Tory, *Phys. Rev. A* **32**, 2347-2351 (1985).
8. S-E Phan and W. B. Russel, *J. Chem. Phys.* **108**, 9789-9795 (1998).
9. J. Tobochnik and P. M. Chapin, *J. Chem. Phys.* **88**, 5824-5830 (1988).
10. Y. Song, R. M. Stratt, and E. A. Mason, *J. Chem. Phys.* **88**, 1126-1133 (1998).
11. M. D. Rintoul and S. Torquato, *Phys. Rev. Lett.* **77**, 4198-4201 (1996).
12. M. Tokuyama and I. Oppenheim, *Phys. Rev. E* **50**, R16-R19 (1994).
13. M. Tokuyama, *Physica A* **289**, 57-85 (2001).
14. M. Tokuyama, *Physica A* **315**, 321-329 (2002).